

# Supernova Nucleosynthesis in the Early Universe

Nozomu Tominaga<sup>1</sup>, Hideyuki Umeda<sup>2</sup>, Keiichi Maeda<sup>3</sup>,  
Ken'ichi Nomoto<sup>3,2</sup>, and Nobuyuki Iwamoto<sup>4</sup>

<sup>1</sup>Optical and Infrared Astronomy Division, National Astronomical Observatory, Mitaka,  
Tokyo, Japan  
email: nozomu.tominaga@nao.ac.jp

<sup>2</sup>Department of Astronomy, School of Science, University of Tokyo, Bunkyo, Tokyo, Japan

<sup>3</sup>Institute for the Physics and Mathematics of the Universe, University of Tokyo, Kashiwa,  
Chiba, Japan

<sup>4</sup>Nuclear Data Center, Nuclear Science and Engineering Directorate, Japan Atomic Energy  
Agency, Tokai, Ibaraki, Japan

**Abstract.** The first metal enrichment in the universe was made by supernova (SN) explosions of population (Pop) III stars. The trace remains in abundance patterns of extremely metal-poor (EMP) stars. We investigate the properties of nucleosynthesis in Pop III SNe by means of comparing their yields with the abundance patterns of the EMP stars. We focus on (1) jet-induced SNe with various energy deposition rates [ $\dot{E}_{\text{dep}} = (0.3 - 1500) \times 10^{51} \text{ergs s}^{-1}$ ], and (2) SNe of stars with various main-sequence masses ( $M_{\text{ms}} = 13 - 50 M_{\odot}$ ) and explosion energies [ $E = (1 - 40) \times 10^{51} \text{ergs}$ ]. The varieties of Pop III SNe can explain varieties of the EMP stars: (1) higher [C/Fe] for lower [Fe/H] and (2) trends of abundance ratios [X/Fe] against [Fe/H].

**Keywords.** Galaxy: halo — gamma rays: bursts — nuclear reactions, nucleosynthesis, abundances — stars: abundances — stars: Population II — supernovae: general

## 1. Introduction

Long-duration  $\gamma$ -ray bursts (GRBs) have been found to be accompanied by luminous and energetic Type Ic supernovae [SNe Ic, called hypernovae (HNe)] (e.g. Galama *et al.* 1998). Although the explosion mechanism is still under debate, photometric observations (a “jet break”, e.g. Frail *et al.* 2001) and spectroscopic observations (a nebular spectrum, e.g. Maeda *et al.* 2002) indicate that they are aspherical explosions with jet(s).

The aspherical explosions are also indirectly suggested from the abundance patterns of extremely metal-poor (EMP) stars with  $[\text{Fe}/\text{H}] < -3$ .<sup>†</sup> The EMP stars are suggested to show nucleosynthesis yields of a single core-collapse SN (e.g. Beers & Christlieb 2005). Particularly, C-enhanced EMP (CEMP) stars have been well explained by the faint SNe with large fallback (Umeda & Nomoto 2005; Iwamoto *et al.* 2005; Nomoto *et al.* 2006; Tominaga *et al.* 2007b). On the other hand, some CEMP stars show enhancement of Co and Zn (e.g. Depagne *et al.* 2002) that requires explosive nucleosynthesis under high entropy. In a *spherical* model, however, a high entropy explosion is equivalent to a high energy explosion that inevitably synthesizes a large amount of  $^{56}\text{Ni}$ , i.e., leads a bright SN (e.g. Woosley & Weaver 1995). This incompatibility will be solved if a faint SN is associated with a narrow jet within which a high entropy region is confined (Umeda & Nomoto 2005).

<sup>†</sup> Here  $[\text{A}/\text{B}] \equiv \log_{10}(N_{\text{A}}/N_{\text{B}}) - \log_{10}(N_{\text{A}}/N_{\text{B}})_{\odot}$ , where the subscript  $\odot$  refers to the solar value and  $N_{\text{A}}$  and  $N_{\text{B}}$  are the abundances of elements A and B, respectively.

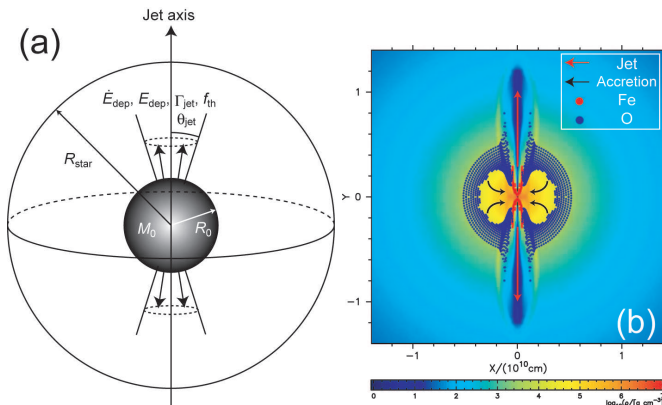


**Figure 1.** (a) Schematic picture of the jet-induced explosion. (b) Density structure of the  $40 M_{\odot}$  Pop III star explosion model of  $\dot{E}_{\text{dep},51} = 15$  at 1 sec after the start of the jet injection.

## 2. Models

We investigate the jet-induced explosions (e.g. Maeda & Nomoto 2003; Nagataki *et al.* 2006) of  $40 M_{\odot}$  Pop III stars (Umeda & Nomoto 2005; Tominaga *et al.* 2007b) using a two-dimensional special relativistic Eulerian hydrodynamic code (Tominaga 2009).

The jets are injected at a radius  $R_0$ , corresponding to an enclosed mass of  $M_0$ , and the jet propagation is followed (Figs. 1ab). Since the explosion mechanism is unknown, the jets are treated parametrically with the following five parameters: energy deposition rate ( $\dot{E}_{\text{dep}}$ ), total deposited energy ( $E_{\text{dep}}$ ), initial half angle of the jets ( $\theta_{\text{jet}}$ ), initial Lorentz factor ( $\Gamma_{\text{jet}}$ ), and the ratio of thermal to total deposited energies ( $f_{\text{th}}$ ).

In particular, we investigate the dependence of nucleosynthesis outcome on  $\dot{E}_{\text{dep}}$  for a range of  $\dot{E}_{\text{dep},51} \equiv \dot{E}_{\text{dep}}/10^{51} \text{ ergs s}^{-1} = 0.3 - 1500$ . The diversity of  $\dot{E}_{\text{dep}}$  is consistent with the wide range of the observed isotropic equivalent  $\gamma$ -ray energies and timescales of GRBs (e.g. Amati *et al.* 2007). Variations of activities of the central engines, possibly corresponding to different rotational velocities or magnetic fields, may well produce the variation of  $\dot{E}_{\text{dep}}$ . We expediently fix the other parameters as  $E_{\text{dep}} = 1.5 \times 10^{52} \text{ ergs}$ ,  $\theta_{\text{jet}} = 15^\circ$ ,  $\Gamma_{\text{jet}} = 100$ ,  $f_{\text{th}} = 10^{-3}$ , and  $M_0 = 1.4 M_{\odot}$  ( $R_0 \sim 900 \text{ km}$ ) in the models.

The hydrodynamical calculations are followed until the homologously expanding structure is reached ( $v \propto r$ ) and then the ejected mass elements are identified from their radial velocities. The nucleosynthesis calculations are performed as post-processing with thermodynamic histories traced with marker particles that represent individual Lagrangian elements. In computing the jet composition, we assume that the jet initially has the composition of the accreted stellar materials.

## 3. Jet-induced Supernovae

### 3.1. Fallback

Figure 2a show “accreted” regions for models with  $\dot{E}_{\text{dep},51} = 120$  and  $1.5 \text{ ergs s}^{-1}$ , where the accreted mass elements initially located in the progenitor. The inner matter is ejected along the jet-axis but not along the equatorial plane. On the other hand, the outer matter is ejected even along the equatorial plane, since the lateral expansion of the shock terminates the infall as the shock reaches the equatorial plane.

The remnant mass ( $M_{\text{rem}}$ ) is larger for lower  $\dot{E}_{\text{dep}}$ . This stems from the balance between the ram pressures of the injecting jet ( $P_{\text{jet}}$ ) and the infalling matter ( $P_{\text{fall}}$ ). In order to

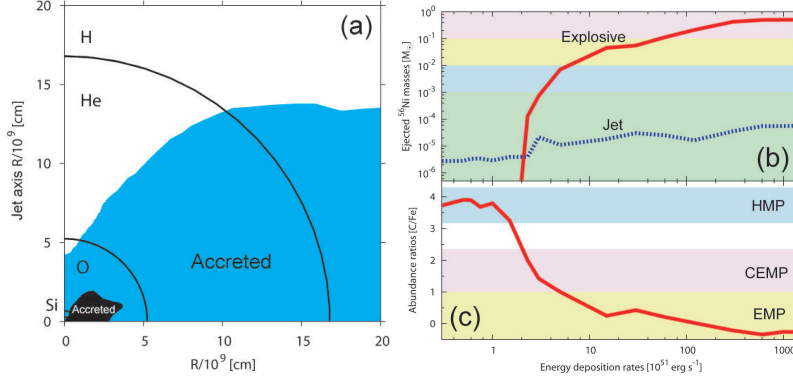


**Figure 2.** (a) Initial locations of the mass elements which are finally accreted for models with  $\dot{E}_{\text{dep},51} = 120$  (black) and with  $\dot{E}_{\text{dep},51} = 1.5$  (cyan). (b) Ejected Fe mass (solid line: explosive nucleosynthesis products, dotted line: the jet contribution) as a function of the energy deposition rate. (c) Dependence of abundance ratio [C/Fe] on the energy deposition rate.

inject the jet,  $P_{\text{jet}}$  should overcome  $P_{\text{fall}}$ .  $P_{\text{jet}}$  is determined by  $R_0$ ,  $\dot{E}_{\text{dep}}$ ,  $\theta_{\text{jet}}$ ,  $\Gamma_{\text{jet}}$ , and  $f_{\text{th}}$ , thus being constant in time in the present models. On the other hand,  $P_{\text{fall}}$  decreases with time, since the density of the outer materials decreases following the gravitational collapse (e.g. Fryer & Mészáros 2003). For lower  $\dot{E}_{\text{dep}}$ ,  $P_{\text{jet}}$  is lower, so that the jet injection ( $P_{\text{jet}} > P_{\text{fall}}$ ) is realized at a later time when the central remnant becomes more massive due to more infall. As a result, the accreted region and  $M_{\text{rem}}$  are larger for lower  $\dot{E}_{\text{dep}}$ .

A model with lower  $\dot{E}_{\text{dep}}$  has larger  $M_{\text{rem}}$ , higher [C/Fe], and smaller amount of Fe [ $M(\text{Fe})$ ] because of the larger amount of fallback (Figs. 2bc, Tominaga *et al.* 2007a). The larger amount of fallback decreases the mass of the inner core relative to the mass of the outer layer. The fallback of the O layer also reduces  $M(\text{Fe})$  because Fe is mainly synthesized explosively in the Si and O layers. The variation of  $\dot{E}_{\text{dep}}$  in the jet-induced explosions predicts that the variation of [C/Fe] corresponds to that of  $M(\text{Fe})$ .

### 3.2. Comparison with the spherical supernova model

The calculations of the jet-induced explosions show that the ejection of the inner matter is compatible with the fallback of the outer matter (Fig. 2a). This is consistent with the two-dimensional illustration of the mixing-fallback model (Fig. 3a) proposed by Umeda & Nomoto (2002). The mixing-fallback model has three parameters; initial mass cut [ $M_{\text{cut}}(\text{ini})$ ], outer boundary of the mixing region [ $M_{\text{mix}}(\text{out})$ ], and a fraction of matter ejected from the mixing region ( $f$ ). The remnant mass is written as

$$M_{\text{rem}} = M_{\text{cut}}(\text{ini}) + (1 - f)[M_{\text{mix}}(\text{out}) - M_{\text{cut}}(\text{ini})]. \quad (3.1)$$

The three parameters relate to the hydrodynamical properties of the jet-induced explosion.

A model with  $\dot{E}_{\text{dep},51} = 120$  and  $M_0 = 2.3M_{\odot}$  ( $R_0 \sim 3 \times 10^3 \text{ km}$ ) is compared with the spherical SN explosion adopting the mixing-fallback model. The inner boundary and the central remnant mass of the jet-induced explosion model are  $M_0 = 2.3M_{\odot}$  and  $M_{\text{rem}} = 8.1M_{\odot}$ . Its abundance pattern is well reproduced by the spherical SN model with the same main-sequence mass  $M_{\text{ms}} = 40M_{\odot}$  and the explosion energy  $E = 3 \times 10^{52}$  ergs (Fig. 3b). The parameters of the mixing-fallback model are  $M_{\text{cut}}(\text{ini}) = 2.3M_{\odot}$ ,  $M_{\text{mix}}(\text{out}) = 10.8M_{\odot}$  and  $f = 0.19$ . The resultant  $M_{\text{rem}}$  ( $= 9.2M_{\odot}$ ) is slightly larger than  $M_{\text{rem}}$  of the jet-induced SN model.

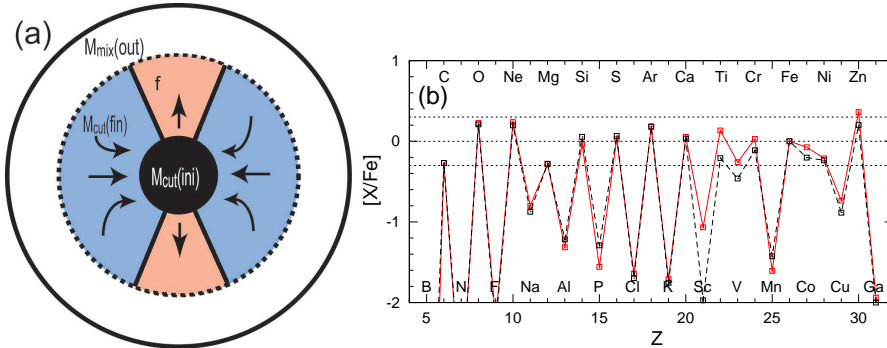


**Figure 3.** (a) Two-dimensional illustration of the mixing-fallback model. (b) Comparison of the abundance patterns of the jet-induced SN model with  $\dot{E}_{\text{dep},51} = 120$  and  $M_0 = 2.3M_{\odot}$  (solid line) and the mixing-fallback model (dashed line).

There, however, are some elements showing differences. The differences stem from the high-entropy explosion due to the concentration of the energy injection (e.g. Maeda & Nomoto 2003). The enhancements of  $[\text{Sc}/\text{Fe}]$  and  $[\text{Ti}/\text{Fe}]$  improve agreements with the observations. Such thermodynamical feature of the jet-induced explosion model cannot be reproduced by the mixing-fallback model, while a “low-density” modification might mimic the high-entropy environment (e.g. Umeda & Nomoto 2005; Tominaga *et al.* 2007b).

#### 4. Trends with Metallicity

The abundance patterns of the EMP stars show certain trends of abundance ratios  $[X/\text{Fe}]$  with respect to  $[\text{Fe}/\text{H}]$  (Cayrel *et al.* 2004). To clarify the origin of the trends, SN models with  $M_{\text{ms}} = 13 - 50M_{\odot}$  are calculated. The explosion energies are set to be consistent with the observations of present SNe (e.g. Tanaka *et al.* 2008).

The abundance ratios against  $[\text{Fe}/\text{H}]$  are compared with yields of individual SN models and the Salpeter’s IMF-integrated yield (Fig. 4).  $[\text{Fe}/\text{H}]$  of a next-generation star is determined by  $M(\text{Fe})$  and a swept-up H mass. Since the swept-up H mass is almost proportional to  $E$  of the SN,  $[\text{Fe}/\text{H}]$  of the next-generation stars are determined by a equation  $[\text{Fe}/\text{H}] = \log_{10} \left[ \frac{M(\text{Fe})}{M_{\odot}} / \left( \frac{E}{10^{51} \text{ergs}} \right)^{6/7} \right] - C$  (Thornton *et al.* 1998), where  $C$  is assumed to be a constant value of 1.4.  $[\text{Fe}/\text{H}]$  of the IMF-integrated abundance ratios are assumed to be the same as SN models with  $E \sim 10^{51} \text{ergs}$  ( $[\text{Fe}/\text{H}] \sim -2.6$ ).

HNe explode with  $E \gtrsim 10^{52} \text{ergs}$  and eject large amount of  $^{56}\text{Ni}$  ( $\gtrsim 0.1M_{\odot}$ ), while normal SNe explode with  $E \sim 10^{51} \text{ergs}$  and eject  $\sim 0.07M_{\odot}$  of  $^{56}\text{Ni}$ . Therefore, according to the above equation,  $[\text{Fe}/\text{H}]$  of a next-generation star originated from a HN is lower than that of a next-generation star originated from a normal SN. The higher-energy explosion raises explosive nucleosynthesis under higher entropy and thus leads higher  $[\text{Zn}/\text{Fe}]$ . This accompaniment explains the observed trends of  $[\text{Zn}/\text{Fe}]$  against  $[\text{Fe}/\text{H}]$ . The trends of other elements are also reproduced by the variations of  $M_{\text{ms}}$  and  $E$  (Fig. 4).

#### 5. Conclusion

We focus on two interesting properties observed in the abundance patterns of the metal-poor stars: (1) the higher  $[\text{C}/\text{Fe}]$  for lower  $[\text{Fe}/\text{H}]$  and (2) the trends of  $[X/\text{Fe}]$  against  $[\text{Fe}/\text{H}]$ . The variations of the metal-poor stars are explained by the variations of SNe

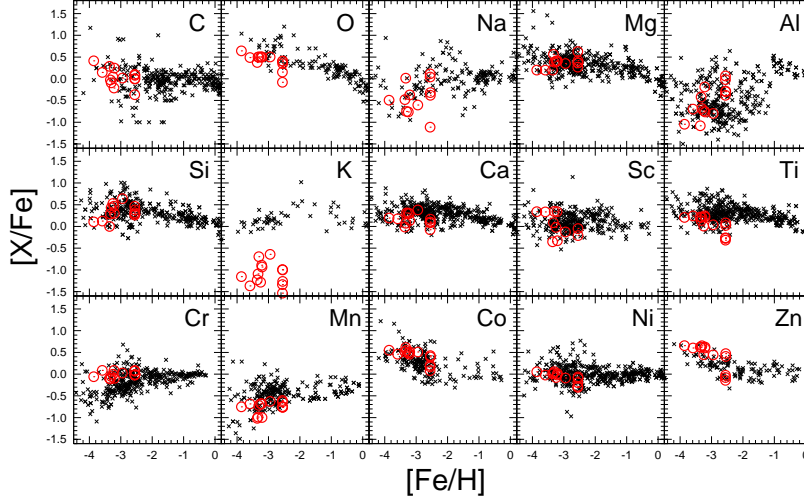


**Figure 4.** Comparison between the  $[X/Fe]$  trends of observed stars (e.g. Cayrel *et al.* 2004; Honda *et al.* 2004: cross) and SN models with the mixing-fallback model and applied the  $Y_e$  and “low-density” modifications (Tominaga *et al.* 2007b: circles).

that contribute the metal enrichment of the early universe. Especially, (1) the variation of the energy deposition rates explains the tendency of  $[C/Fe]$  against  $[Fe/H]$  and (2) the variations of  $M_{ms}$  and  $E$  explain the trends of  $[X/Fe]$  against  $[Fe/H]$ . We propose that the abundance patterns of the metal-poor stars will provide additional constraints on the explosion mechanism of GRBs and SNe other than the direct observations of present GRBs and SNe.

This work has been supported in part by WPI Initiative, MEXT, Japan.

## References

- Amati, L., Della Valle, M., Frontera, F., *et al.* 2007, *A&A*, 463, 913  
 Beers, T.C., & Christlieb, N. 2005, *ARAA*, 43, 531  
 Cayrel, R., Depagne, E., Spite, M., *et al.* 2004, *A&A*, 416, 1117  
 Depagne, E., Hill, V., Spite, M., *et al.* 2002, *A&A*, 390, 187  
 Frail, D.A., Kulkarni, S. R., Sari, R., *et al.* 2001, *ApJ* (Letters), 562, L55  
 Fryer, C., & Mészáros, P. 2003, *ApJ* (Letters), 588, L25  
 Galama, T. J., Vreeswijk, P. M., van Paradijs, J., *et al.* 1998, *Nature*, 395, 670  
 Honda, S., Aoki, W., Kajino, T., *et al.* 2004, *ApJ*, 607, 474  
 Iwamoto, N., Umeda, H., Tominaga, N., Nomoto, K., & Maeda, K. 2005, *Science*, 309, 451  
 Maeda, K., Nakamura, T., Nomoto, K., *et al.* 2002, *ApJ*, 565, 405  
 Maeda, K., & Nomoto, K. 2003, *ApJ*, 598, 1163  
 Nagataki, S., Mizuta, A., & Sato, K. 2006, *ApJ*, 647, 1255  
 Nomoto, K., Tominaga, N., Umeda, H., *et al.* 2006, *Nucl. Phys. A*, 777, 424 (astro-ph/0605725)  
 Tanaka, M., Tominaga, N., Nomoto, K., *et al.* 2008, *ApJ*, submitted (arXiv:0807.1674)  
 Thornton, K., Gaudlitz, M., Janka, H.-Th., & Steinmetz, M. 1998, *ApJ*, 500, 95  
 Tominaga, N., Maeda, K., Umeda, H., *et al.* 2007a, *ApJ* (Letters), 657, L77  
 Tominaga, N., Umeda, H., & Nomoto, K. 2007b, *ApJ*, 660, 516  
 Tominaga, N. 2009, *ApJ*, in press (arXiv:0711.4815)  
 Umeda, H., & Nomoto, K. 2002, *ApJ*, 565, 385  
 Umeda, H., & Nomoto, K. 2005, *ApJ*, 619, 427  
 Woosley, S. E., & Weaver, T. A. 1995, *ApJS*, 101, 181